Journal of Spatial Information Sciences

...JSIS

EVALUATING THE CONSISTENCY OF GNSS REPEAT MEASUREMENTS: AN INVESTIGATION INTO THE EFFECTS OF ORBITAL ERRORS ON SAME-TIME, SAME-DATE OBSERVATIONS IN DIFFERENT YEARS IN ABUJA, NIGERIA

ATOKI Lucas Olu, BURAIMOH Korede Samuel, SANGOTOYE Ololade Ayotunde, EDOKI Echeng Isaac

JOURNAL OF SPATIAL INFORMATION SCIENCES ISSN: 2354-3361
VOL. 2, ISSUE 1, PP 189–205, 2025 **DOI:** https://doi.org/10.5281/zenodo.14947243
PUBLISHED 28-02-2025

www.journals.unizik.edu.ng/jsis

EVALUATING THE CONSISTENCY OF GNSS REPEAT MEASUREMENTS: AN INVESTIGATION INTO THE EFFECTS OF ORBITAL ERRORS ON SAME-TIME, SAME-DATE OBSERVATIONS IN DIFFERENT YEARS IN ABUJA, NIGERIA

[1]ATOKI Lucas Olu, [2]BURAIMOH Korede Samuel, [3]SANGOTOYE Ololade Ayotunde, [4]EDOKI Echeng Isaac

Department of Surveying and Geoinformatics, Bowen University, Iwo, Osun State, Nigeria.

Corresponding Author: [1]lucas.atoki@bowen.edu.ng

DOI: https://doi.org/10.5281/zenodo.14947243

Abstract

High-accuracy satellite orbits and clock synchronization are vital for the International GNSS Service, supporting precise urban mapping and infrastructural development. However, by treating the predicted orbits as fixed, the orbital errors may be partially assimilated by the estimated satellite clock and hence impact the positioning solutions. This study presents the evaluation of the consistency of GNSS repeat measurements, taking interest in the investigation of the effects of orbital errors on same-time same-date observations in different years in Abuja, Nigeria. The study adopts the determination of the GNSS Static observations (minimum of two hours per session) on the chosen stations, investigation of the impact of GNSS orbital errors on repeat measurements, analyzing and characterizing sources of variability in repeated measurements. Our study shows that precise repeat observations can be attained by thoroughly mitigating errors from other observable sources, enabling reliable detection and management of recurring geodetic deformations in deformation monitoring. The RMSE values of 0.040m for both approaches demonstrate that the observations from both years exhibit comparable levels of precision and accuracy, meeting geodetic positional certainty standards. Therefore, it is recommended to perform observations with scrupulous care to eliminate other error sources impacting the precision of positional data.

Key Words: IGS, PPP, GNSS, Consistency, orbital errors, Repeat Measurements.

1.0 Introduction

Precise satellite positioning and timing, enabled by accurate orbits and clocks, are essential for the International GNSS Service to support smart urban planning and development [2]; [29]. As described by [23], a satellite is essentially a self-contained unit that facilitates communication by receiving signals from Earth and rebroadcasting them via an integrated transponder. To reach orbit, a satellite must endure intense acceleration during launch, achieving speeds of 28,100 km/h (17,500 mph), and then withstand harsh space conditions, including radiation and extreme temperatures, for up to 20 years. Satellites require lightweight designs to minimize launch costs, which are weight-dependent. To achieve this, satellites are constructed with compact, durable materials, ensuring reliability exceeding 99.9% in space. Key components include communication, power, and propulsion systems. Achieving high-precision Precise Point Positioning (PPP) requires accurate satellite orbit and clock data, a critical factor in obtaining precise location results as detailed by [38]. The International GNSS Service (IGS) has been producing precise GPS satellite orbit and clock products since 1994, combining data from multiple analysis centers, including Center for Orbit Determination in Europe (CODE), GeoForschungsZentrum (GFZ), and Jet Propulsion Laboratory (JPL) as expressed by [15]. A range of products with varying accuracy and latency are available to cater to diverse application requirements, including the IGS final products, which provide the highest accuracy for scientific purposes, with 15-minute orbit and 30-second clock solution sampling intervals opined by [18]

Although IGS final products offer high accuracy, their 12-18 day latency restricts their use in real-time applications, whereas IGS ultra-rapid products provide 48-hour orbit and clock solutions at 15-minute intervals. Ultra-rapid products comprise two parts: the first 24 hours are estimated from recent GPS observational data, while the second half consists of predicted orbits and clock solutions, updated every six hours with a three-hour delay as depicted by [26].

In 2007, the International GNSS Service (IGS) invited participation in a real-time pilot project, focusing on generating and disseminating real-time clocks among other key objectives [36]; [10]. Furthermore, recent research has focused on integrating satellite uncalibrated Phase Delays (UPDs) and ionospheric products with real-time clocks in GNSS augmentation systems to achieve enhanced accuracy, particularly for regional services [24]. Fixing predicted satellite orbits affects estimated clock solutions due to inherent orbit errors. GPS predicted ultra-rapid orbits typically achieve ~5 cm accuracy over 24 hours, but degrade to several decimeters during eclipses, mainly due to satellite yaw-attitude issues in older GPS satellites as opined by [26]. The issue is more pronounced for newer navigation satellite systems like BeiDou, where precise orbit solutions are less accurate than GPS due to the utilization of Geostationary Orbit (GEO) and Inclined Geosynchronous Orbit (IGSO) satellites, regional tracking networks, and specific processing strategies, with reported orbit accuracy ranging from 10-20 cm [36].

Estimating satellite clocks using these orbit products will likely introduce errors, potentially biasing positioning results, although some orbital errors can be mitigated by the estimated satellite clocks. [26] conducted an impact analysis of radial and tangential orbital errors on satellite clock estimation and Precise Point Positioning (PPP), exploring the theoretical and experimental effects of orbital error compensation by satellite clocks and satellite-station geometry. Research using regional station networks of varying sizes (~100, ~300, ~500, and ~700 km radius) revealed that orbital errors absorbed by satellite clock estimates decrease as network size increases. A novel regional PPP approach leveraging broadcast ephemeris and estimated satellite clocks was proposed and assessed through numerical analysis.

Research revealed that orbital errors in broadcast ephemeris have minimal impact on Precise Point Positioning (PPP) users within a 300 km regional network, achieving positioning RMS of 1.4, 1.4, and 3.7 cm (east, north, up) in post-mission kinematic mode, comparable to results using precise orbits and estimated clocks (1.3, 1.3, 3.6 cm). This paper investigates and evaluates the consistency of GNSS repeat measurements, taking interest in the investigation of the effects of orbital errors on same-time same-date observations in different years in Abuja, Nigeria.

1.1 Study Area

The research work was carried out in Abuja, FCT, Nigeria. The area is geographically located at the north central part of Nigeria. It falls between latitude 8.05515211N, 9.0113411N and longitude 6.05113611E, 7.01113511E (fig.1.1).

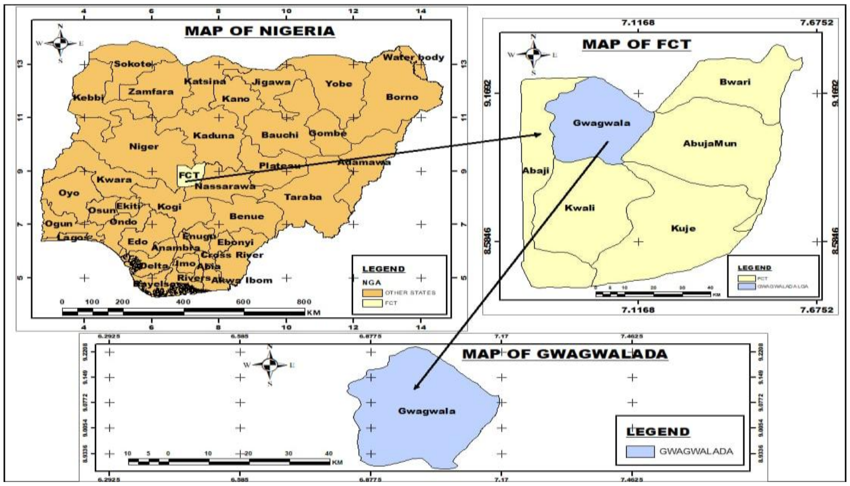

Fig. 1.1: Study area in Gwagwalada, Nigeria.

2.1 Consistent Urban Positioning and Digital Mapping

The increasing pace of urbanization underscores the importance of investigating ways to optimize the safety and efficiency of utility network construction and operation, driving this research endeavor, [33] The objective of this research is to evaluate the consistency of GNSS measurements over time, focusing on the influence of orbital errors on observations made at identical times and dates in different years. [27] employed a multi-faceted approach, incorporating analytical, classification, functional, statistical, and synthesis methods. A Research by [22] highlights the limitations of GNSS/INS-RTK systems in mapping complex environments due to signal obstruction and deflection, questioning the reliability of commercial mapping solutions relying on these expensive systems. Urban canyons and dense infrastructure can severely impact GNSS positioning, leading to errors of up to 10 meters, as satellite signals are obstructed and reflected by surrounding structures. Integrating Three-Dimensional (3D) building maps can substantially enhance positioning accuracy. Research by [1] presents a novel integration of GNSS shadow matching and 3D-mapping-aided ranging, leveraging direction-dependent weighting to combine position solutions. They evaluate two weighting strategies for integrating GNSS shadow matching and 3D-mapping-aided ranging: one based on error covariance matrices and another using street azimuth. Experimental results from a u-blox GNSS receiver demonstrate that both combined solutions significantly outperform individual shadow matching or 3D-mapping-aided ranging in terms of accuracy. The covariance-based weighting approach achieved an impressive Root Mean Square (RMS) horizontal accuracy of 6.1 meters, representing a four-fold improvement over conventional GNSS positioning, which yielded an accuracy of 25.9 meters. [35]; [25] demonstrate the effectiveness of integrating shadow matching with traditional GNSS positioning using smartphone data, showcasing promising results.

Fig. 2.1: representation of mapping challenges [1]

2.2 The effects of satellite orbital inaccuracies

This section examines the impact of satellite orbital errors on Precise Point Positioning (PPP) accuracy and satellite clock estimation, using mathematical models outlined by [28]. Under the assumption of fixed, known station coordinates and satellite orbits, the observation equations for ionosphere-free pseudorange and phase combinations can be linearized as;

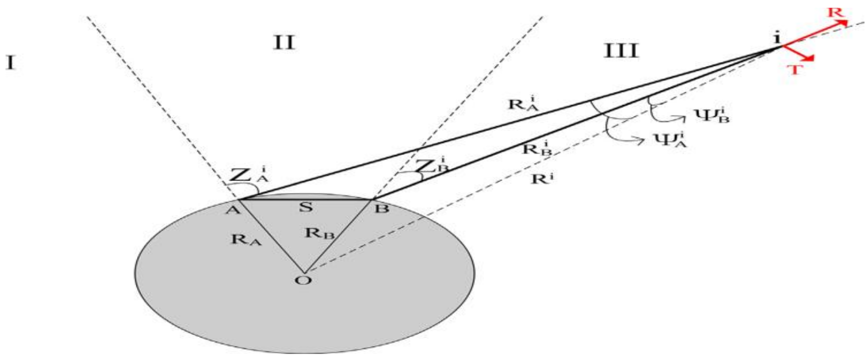

Fig. 2.2**:** Representation of Orbital Error Components [28].

ISSN: 2354-3361
VOL. 2, ISSUE 1, PP 189–205, 2025 DOI: https://doi.org/10.5281/zenodo.14947243
PUBLISHED 28-02-2025
www.journals.unizik.edu.ng/jsis

[26] illustrated the decomposition of Orbital Errors for Satellite i into Radial (R) and Tangential (T) Components at Stations A and B, separated by Distance S, with Sky Regions Divided into I, II, and III.

$$PiA = RiA + \frac{RiA}{RiA}.\Delta Xi + c \cdot tA - c \cdot ti + miA.ZTD + eiA \quad \text{.................... Equ. 2.1}$$

$$LiA = RiA + \frac{RiA}{RiA}.\Delta Xi + c \cdot tA - c \cdot ti + miA.ZTD - \lambda.NiA + \varepsilon iA \quad \text{............... Equ. 2.2}$$

PiA and LiA represent ionosphere-free pseudorange and phase observations from receiver A to satellite i.; RiA represents the geometric distance between receiver A and satellite i, accounting for relativity effects, phase wind-up, antenna phase center corrections, and ocean loading; ΔXi symbolizes the orbital error of satellite i; tA and ri represent receiver and satellite clock biases; c is the vacuum speed of light; ZTD represents the zenith tropospheric delay, while m^iA is its associated mapping function; λ represents the wavelength, and N^iA denotes the ambiguity of the ionosphere-free phase measurement; eiA and eiA represent the noise terms for pseudorange and phase observations, respectively; and R^iA/R^iA. ΔXi is the scalar projection of orbital errors along the line-of-sight between satellite and receiver. Given the vast distance (>20,000 km) between satellite and receiver, small orbital errors (<1 km) have negligible effect on mapping function miA. Figure 2.2 illustrates the decomposition of orbital error projections on range measurements into radial and tangential components, and R^iA/RiA. ΔX^i can be denoted as;

$$\frac{RiA}{RiA}.\Delta Xi = \cos \Psi iA.\Delta XiR + \sin\Psi iA.\Delta XiT \quad \text{.................. Equ.2.3}$$

where ΔX^i_R denotes orbital errors in the radial component; ΔXi_T denotes the tangential orbital error that represents the projection of combined errors in the along-track and cross-track components on Plane oAi as represented in Fig. 2.2. The tangential orbital error ΔXiT is influenced by errors in along-track and cross-track components, as well as the satellite's track orientation relative to the receiver; ΨiA represents the parallax angle of satellite i as viewed from receiver A and the Earth's center [9]. It can be represented as a function of the angle between the satellite and the local zenith:

$$\Psi iA = \arcsin\left(\frac{RA\ .\sin ZiA}{Ri}\right) \quad \text{................ Equ.2.4}$$

where R_A and R^i denote the geocentric distance of receiver A and satellite i, respectively; Z^i_A denotes the zenith distance of satellite i. If we let $R_A \approx 6371$ km and $R^i \approx (20200 + RA)$ km, the range of Ψ^i_A is between 0^o and 13.9^o. Carrier-phase measurements' ambiguity necessitates pseudorange measurements to determine absolute clock offsets, whereas carrier-phase governs epoch-wise clock accuracy as detailed by [26].

2.3 A broadcast orbit using the RTS satellite position correction

[11] pointed out the viable efforts of the International GNSS Service (IGS) at ensuring the precise GPS satellite orbit and clock corrections which are available in real-time service. These products are known as the IGS-Real Time Service (IGS-RTS) and the precision and accuracy of IGS orbits as was explained by [18]. Also, [3]; [32], ascertained the maintenance of real-time precise point positioning during outages of orbit and its clock corrections as represented in the table 2.2.
As opined by [37], RTS orbit correction is given in the form of radial, along-track, and cross-track (RAC) elements. The mathematical update of the GNSS broadcast message using the IGS-RTS

correction data is described as follows; A broadcast orbit using the RTS satellite position ($\delta\vec{X}$) correction can be corrected as

$$\vec{X}_{\text{Orbit}} = \vec{X}_{\text{broadcast}} - \delta\vec{X} \tag{2.1}$$

Where $\delta\vec{X}$ is the RTS satellite position correction expressed in earth-centered earth-fixed (ECEF) coordinates, $\vec{X}_{\text{orbit}}$ is the satellite position vector corrected by the RTS correction, and $\vec{X}_{\text{broadcast}}$ is the satellite position vector computed from GNSS broadcast ephemeris. The raw RTS correction data is expressed in radial, along-track, and cross-track (RAC) coordinates, also the broadcast orbit is expressed in ECEF coordinates. According to [13], the discrepancies necessitate converting corrections from Radiation Angle Coordinate (RAC) to Earth-Centered Earth-Fixed (ECEF) coordinate system. The unit vectors $\vec{r}$ representing the Radiation Angle Coordinate (RAC) components can be calculated from the broadcast position (r) and velocity vectors ($\dot{\vec{r}}$) as;

$$\vec{e}_{\text{Along}} = \frac{\dot{\vec{r}}}{[\vec{r}]},\ \vec{e}_{\text{cross}} = \frac{\vec{r} \times \dot{\vec{r}}}{[\vec{r} \times \dot{\vec{r}}]},\quad \vec{e}_{\text{radial}} = \vec{e}_{\text{along}} \times \vec{e}_{\text{cross}} \tag{2.2}$$

$$\delta\vec{X}\ (t) = [\vec{e}_{\text{radial}}, \vec{e}_{\text{along}}, \vec{e}_{\text{cross}}]\ \delta\vec{O}\ (t), \tag{2.2a}$$

where $\vec{e}_{\text{radial}}$, $\vec{e}_{\text{along}}$, and $\vec{e}_{\text{cross}}$ are the unit vectors for radial, along-track, and cross-track coordinates, respectively $\delta\vec{O}\ (t)$ is the orbit correction represented in RAC coordinates. All the correction components consist of transmitted orbit correction, δO_i, and its rate of change, $\delta\dot{O}_i$, as

$$\delta O_i\,(t) = \delta\ (t_0) + \delta\dot{O}_i\ (t - t_0) \tag{2.3}$$

Where $_i$ = radial, along-track, and cross-track, also t is the current time to compute the correction, and t_0 is the time of applicability that is included in the RTS message.

The RTS clock correction, δC (t), is given as a correction to the broadcast clock offset. And for the orbit correction, the clock correction consists of the transmitted correction and its rate of change:

$$\delta C\ (t) = C_0 + C_1\,(t - t_0) + C_2\,(t - t_0)^2 \tag{2.4}$$

Where C_0, C_1, and C_2 represent the transmitted clock corrections. (t) is expressed as a correction-equivalent range unit, and where $\delta t\ (t)$ is expressed as the clock offset, which can be obtained by dividing it by the speed of light c:

$$\delta t\ (t) = (\delta C\ (t) c\ )/c \tag{2.5}$$

Table2.1: A broadcast orbit using the RTS satellite position correction [20]

Product	**Parameter**	**Accuracy**	**Latency**
Real-time service (RTS)	Orbit Clock	5cm 0.5ns	25s
Ultra rapid(predicted)	Orbit Clock	10cm 5ns	Real-time
Ultra rapid(estimated)	Orbit Clock	3cm 0.2ns	3hrs
Rapid (estimated)	Orbit Clock	2.5cm 0.10ns	7hrs
Final (estimated)	Orbit Clock	2cm <0.10ns	14 days

JOURNAL OF SPATIAL INFORMATION SCIENCES ISSN: 2354-3361
VOL. 2, ISSUE 1, PP 189–205, 2025 DOI: https://doi.org/10.5281/zenodo.14947243
PUBLISHED 28-02-2025
www.journals.unizik.edu.ng/jsis

2.4 Precise Point Positioning (PPP)

Precise Point Positioning (PPP) has been affirmed as a valuable method for single point positioning which can be used all over the globe. PPP has also become a viable technique that can give an accurate positioning with just a single receiver. Also where the installation of a reference station for RTK could be difficult or simply too expensive, PPP is usually used in such environment. However, a clear-horizon environment is recommended as it is very sensitive to cycle slip. It consists in using precise orbits and clock products, as it is freely available on the IGS website or using private companies such as satellite link with Navcom Technology, which are considered as fundamental corrections for systematic satellite orbit and clock errors that cannot be modeled. [22]; [21]. One serious problem for real-time PPP applications such as natural hazard early warning systems and surveying is when a sudden communication break takes place resulting in a discontinuity in receiving these orbit and clock corrections for a period that may extend from a few minutes to hours as opined by [14]; [12]. The mathematical model for PPP as described by [11] involves two observation equations as explained below:

$$P_{iono\text{-}free} = \rho + c\,(dt - dT) + T + \varepsilon_P \quad \text{……… (2.14)}$$

$$\varphi_{iono\text{-}free} = \rho + c\,(dt - dT) + T + N\lambda + \varepsilon_\varphi \quad \text{…………. (2.15)}$$

where $P_{iono\text{-}free}$ and $\varphi_{iono\text{-}free}$ are ionosphere free combination of L1 and L2 for pseudorange and carrier-phase measurements respectively, ρ is the geometric range between satellite and station, c is the vacuum speed of light, dt and dT are receiver and satellite clock offset that can be corrected by the employed precise clock products, respectively, T is the tropospheric delay, N is the float ambiguity and ε_P and ε_L are the relevant measurement noise, including satellite orbit residual error, multipath error and other un-modeled errors as detailed by [6]. Geometric range is a function of the satellite coordinates (XS, YS, ZS) that their accuracies are affected by the employed precise orbits products and the receiver coordinates (xr, yr, zr) that are considered as unknown parameters in the PPP estimator, which can be described by the following equation:

$$\rho = \sqrt{(X^S - x_r)^2 + (Y^S - y_r)^2 + (Z^S - z_r)^2} \quad \text{………(2.16)}$$

Recently, going by the illustration given by [16], the IGS has been providing an accurate GPS satellite orbits and clock corrections for real-time applications. [30] highlight IGS-RTS as a reliable source of accurate real-time products, utilizing a network of over 130 globally distributed GPS stations to estimate satellite orbits and clock corrections, with corrections delivered through NTRIP.

3.0 Methodology

A work flow-diagram for the research methodology.

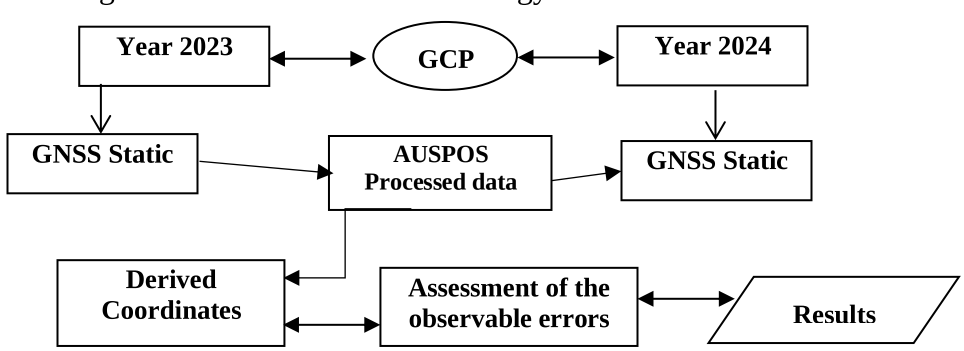

Figure 3.1: A flowchart of the design.

3.1 GNSS Static Positioning Approach

A unit of Hi-Target 90 GNSS dual-frequency receiver was employed for static observations at six Ground Control Point (GCP), with technical specifications outlined in Table 3.1. After verifying the receiver's functionality, observations were conducted for a minimum of two hours at each GCP between July 18-19, 2023 (DOY 199-200). The receiver was set to collect data at 15-second intervals with a mask angle of 15°. The observed data was converted to RINEX format [19] and submitted for online processing on August 13, 2023 (DOY 225), using AUSPOS 2.4, which utilizes IGS products to compute precise coordinates in the International Terrestrial Reference Frame (ITRF). AUSPOS employs the Bernese GNSS Software Version 5.2 for data processing. All data was optimally processed, and positions were determined in ITRF14.

Table 3.1: Technical Specifications of GPS Receivers

ITEM	**HI-TARGET V90+ GPS RECEIVER**
Type	Dual frequency
Channels	220 Channels (GPS, GLONASS, SBAS, GALILEO, BDS, QZSS)
Ports	1 mini USB, 1 5-pin serial for NMEA output, external devices, power, etc
Bluetooth	Dual mode BT4.0
Kinematic Accuracies	Horizontal: 10mm + 1ppm RMS Vertical: 2.5mm + 1ppm RMS **RTK:** Hor.: 8mm+1ppm; Vert.: 15mm+1ppm
Static Accuracies	Horizontal: 2.5mm + 1ppm RMS Vertical: 5mm + 1ppm RMS
Transmission/ Reception Formats	CMR, CMR+, sCMRx RTCM: 2.1, 2.3, 3.0, 3.1, 3.2
DGPS	NMEA 0183GSV, AVR, RMC, HDT,VGK, VHD, ROT, GGK, GGA, GSA, ZDA, VTG, GST, PJT, PJK, etc
Communication (Data Links)	Radio modem, Internal 3G, compatible with GPRS, GSM, and Network RTK

3.3 Analyzing and Characterizing Sources of Variability in Repeated Measurements.

The following analysis are based on the Australia online post processing outcomes [7]
Data preprocessing: Phase preprocessing is undertaken in a baseline by baseline mode using triple-difference. In most cases, cycle slips are fixed by the simultaneous analysis of different linear combinations of L1 and L2. If a cycle slip cannot be fixed reliably,bad data points are removed or new ambiguities are set up A data screening step on the basis of weighted post-fit residuals is also performed, and outliers are removed.
Basic observable: Carrier phase with an elevation angle cutoff of 7° and a sampling rate of 3 minutes. However, data cleaning is performeda sampling rate of 30 seconds. Elevation dependent weighting is applied according to $1/\sin(e)^2$ where e is the satellite elevation.
Modelled observable: Double differences of the ionosphere-free linear combination.
Ground antenna phase center calibration: IGS14 absolute phase-center variation model is applied.

Tropospheric Model: A priori model is the GMF mapped with the DRY-GMF.
Tropospheric Estimation: Zenith delay corrections are estimated relying on the WET-GMF mapping function in intervals of 2-hour. N-S and E-W horizontal delay parameters are solved for every 24 hours.
Tropospheric Mapping Function: GMF
Ionosphere: First-order effect eliminated by forming the ionosphere-free linear combination of L1 and L2. Second and third effect applied.
Tidal displacements: Solid earth tidal displacements are derived from the complete model from the IERS Conventions 2010, but ocean tide loading is not applied.
Atmospheric loading: Applied Satellite center of mass correction: IGS14 phase-center variation model applied.
Satellite phase- center calibration: IGS14 phase-center variation model applied
Satellite trajectories: Best available IGS products.
Earth Orientation: Best available IGS products.
Adjustment: Weighted least-squares algorithm.
Station coordinates: Coordinate constraints are applied at the Reference sites with standard deviation of 1mm and 2mm for horizontal and vertical components respectively.
Ambiguity: Ambiguities are resolved in a baseline-by-baseline mode using the Code-Based strategy for 200-6000km baselines, the Phase-Based L5/L3 strategy for 20-200km baselines, the Quasi-Ionosphere-Free (QIF) strategy for 20-2000km baselines and the Direct L1/L2 strategy for 0-20km baselines.

4.0 Results and Discussions

4.1 Results for Differential GNSS Static Positioning done at Year 2023

The results of the differential GNSS static positioning done with Hi-Target V90 GNSS dual frequency receiver was converted into RINEX [19] format and processed online by AUSPOS with Bernese software v5.2 (Table 4.1). The Cartesian (X, Y, Z) and geodetic (latitude ϕ, longitude λ and ellipsoidal height h) coordinates of the six ground control points (AB1, AB2, AB3, AB4, AB5 and AB6) were given in ITRF 2014 datum [5]. Out of all the IGS reference stations (ADIS, ASCG, CPVG, DYNG, EBRE, LPAL, MAS1, MAT1, NKLG, SFER, STHL, VILL, WIND and YEBE) used for the processing, NKLG is the nearest to the study area with a baseline length of about 990km. Hence, it is the reference station used to form baselines with the stations in the network by AUSPOS.

Table4.1: ITRF2014 Coordinates from GNSS Static method processed by AUSPOS

ID	ITRF 2014 COORDINATES (2023 observations)						Ambiguity Resolution	**18/07/2023 (DoY=199)**	
	CARTESIAN (m)			Positional Uncertainty (±2σ)					
	X (m)	Y (m)	Z (m)	ϕ (±m)	λ (±m)	h (m)			
							(%)	Start Time	End Time
AB1	6252855.907	778709.082	986131.768	± 0.010	± 0.026	±0.041	60.0	07:23:30	09:40:30

JOURNAL OF SPATIAL INFORMATION SCIENCES ISSN: 2354-3361
VOL. 2, ISSUE 1, PP 189–205, 2025 **DOI:** https://doi.org/10.5281/zenodo.14947243
PUBLISHED 28-02-2025
www.journals.unizik.edu.ng/jsis

AB2	6252867.431	778887.668	985906.155	± 0.012	± 0.022	± 0.051	69.2	09:59:30	12:15:30
AB3	6252883.247	778999.713	985709.506	± 0.024	± 0.012	±0.049	58.4	01:28:30	15:33:30
								19/07/2023 (DoY=200)	
AB4	6252830.952	779255.835	985836.153	± 0.019	± 0.010	±0.050	54.5	07:58:30	10:04:00
AB5	6252749.708	779693.683	985930.584	± 0.025	± 0.011	±0.055	75.0	10:30:30	12:55:30
AB6	6252939.977	778711.975	985560.110	± 0.030	± 0.012	±0.062	54.6	15:47:00	17:51:30

The percentage (%) ambiguity resolution (A.M.) of the solution indicates the success rate of the processing. Fifty percent (50%) or better for a baseline indicates a reliable solution (AUSPOS Report, 2023). For all the GCPs, the success rates were greater than 55% except for station AB4 and AB6 (54.5% and 54.6% respectively).

Geodetic positional uncertainties of the GCPs were determined at 95% confidence limit (according to the processing report from [7]. The mean horizontal error and vertical error were computed respectively as follows;

$$\text{rms vertical error} = \sqrt{\frac{\sum_{i=1}^{n}(\Delta U^2)i}{n}} \qquad (4.1)$$

$$2 - \text{D rms horizontal error} = \sqrt{\frac{\sum_{i=1}^{n}(\Delta E i^2 + \Delta N i^2)}{n}} \qquad (4.2)$$

The mean uncertainties for horizontal and vertical positions are ±0.027m and ±0.052m respectively; while the maximum are ±0.030m and ±0.062m respectively.

4.2 Results for Differential GNSS Static Positioning done at Year 2024

The results of the differential GNSS static positioning done with Hi-Target V90 GNSS dual frequency receiver and processed online by AUSPOS with Bernese software v5.2 (Table 4.2). The Cartesian (X, Y, Z) and geodetic (latitude ϕ, longitude λ and ellipsoidal height h) coordinates of the six ground control points (AB1, AB2, AB3, AB4, AB5 and AB6) were given in ITRF 2014 datum [5]. Out of all the IGS reference stations (ASCG, DYNG, EBRE, LPAL, MAS1, MAT1, NKLG, STHL, VILL, WIND) used for the processing, NKLG is the nearest to the study area with a baseline length of about 990km. Hence, it was also the reference station used to form baselines with the stations in the network by AUSPOS.

Table4.2: ITRF2014 Coordinates from GNSS Static method processed by AUSPOS

ID	ITRF 2014 COORDINATES(2023 observations)						Ambiguity Resolution	**18/07/2024 (DoY=200)**	
	CARTESIAN (m)			Positional Uncertainty (±2σ)					
	X (m)	Y (m)	Z (m)	ϕ (±m)	λ (±m)	h (m)			
							(%)	Start Time	End Time
AB1	6252855.850	778709.091	986131.750	± 0.015	± 0.020	±0.050	70.0	07:23:29	09:40:12
AB2	6252867.425	778887.668	985906.182	± 0.019	± 0.045	± 0.116	50.0	09:59:30	12:15:21
AB3	6252883.235	778999.736	985709.494	± 0.024	± 0.038	±0.058	63.6	01:28:31	15:33:38
								19/07/2024 (DoY=201)	

AB4	6252831.100	779255.921	985836.179	± 0.011	± 0.021	±0.059	75.0	07:58:11	10:04:02
AB5	6252749.657	779693.694	985930.587	± 0.010	± 0.014	±0.050	63.6	10:30:28	12:55:39
AB6	6252939.986	778711.940	985560.102	± 0.014	± 0.029	±0.048	66.6	15:47:09	17:51:10

The percentage (%) ambiguity resolution (A.M.) of the solution indicates the success rate of the processing, [8]. For all the GCPs, the success rates were greater than 55% except for station AB2 (50.0%), [31]. The mean uncertainties for horizontal and vertical positions are ±0.034m and ±0.068m respectively; while the maximum are ±0.045m and ±0. 0.116m respectively.

4.3 Assessment of the GNSS repeat observations

Table 4.3: The difference in coordinates of 2023 and 2024 observations

ID	ΔX	ΔY	ΔZ	3-D Error
AB1	0.057	0.009	0.018	0.061
AB2	0. 006	0.000	0.027	0.028
AB3	0.012	0.023	0.012	0.029
AB4	0.148	0.086	0.026	0.173
AB5	0.051	0.011	0.003	0.052
AB6	0.009	0.035	0.008	0.037
	RMS Discrepancy = 0.040			

$$\text{RMS} = \sqrt{\frac{\sum_{i=1}^{n}(\Delta x)2}{\mathbf{n}}} \tag{4.3}$$

An analysis of Tables 4.1-4.3 and Fig. 4.1 reveal that station AB2's data collected between 09:59:30 GMT and 12:15:30 GMT shows precise x, y, and z axis values of 0.006m, 0.000m, and 0.027m, closely matching the actual values. With a 0.000m y-axis error and 3D error of 0.028m, the lowest among six stations, station AB2 demonstrates optimal precision, supporting repeat measurement reliability, contingent on mitigation of other observable errors. Analyzing the variations in geodetic positional uncertainties among coordinate observations at each station, despite utilizing advanced international models to quantify observable errors, complete elimination proved unfeasible, yet significant mitigation was achieved.

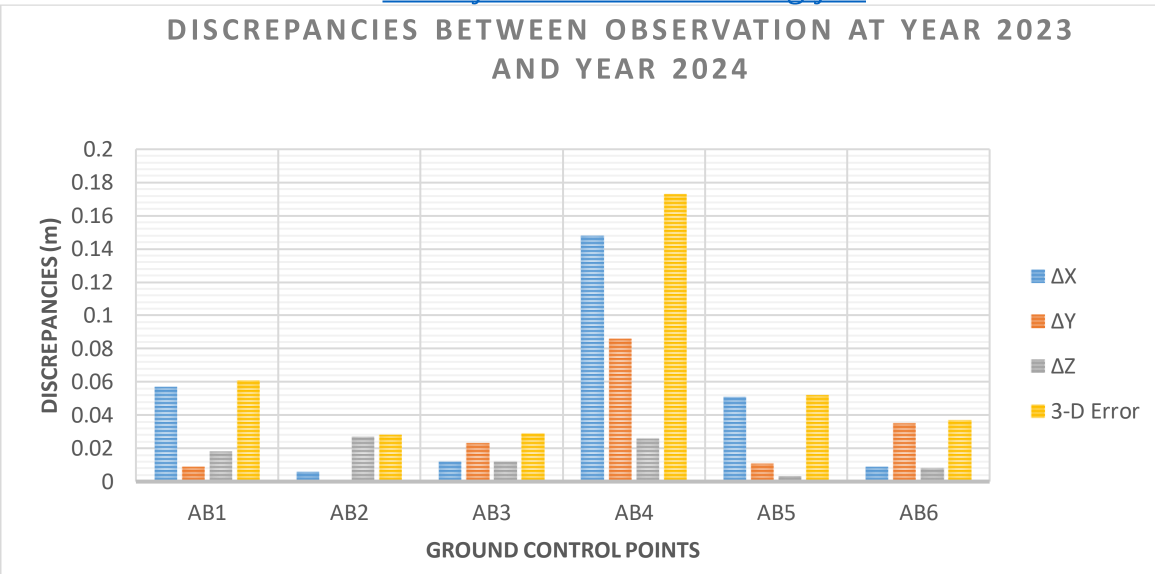

Fig4.1: Representation of the Discrepancies between observation of Year 2023 and Year 2024

According to the AUSPOS report [8], ambiguity resolution employs distinct strategies based on baseline length: Code-Based (200-6000km), Phase-Based L5/L3 (20-200km), Quasi-Ionosphere-Free (20-2000km), and Direct L1/L2 (0-20km), yet results exhibit variability in ambiguity resolution across stations check [31]; [17]. This therefore contributed to the impossibility of getting exact values for the repeat observations. The RMSE values of 0.040m for both methods demonstrate that the observations from both years exhibit comparable levels of precision and accuracy, meeting geodetic positional certainty standards.

Field Speed: Static GNSS field observations were conducted for at least two hours at each ground control point, repeated at each year. The high degree of agreement (<4cm) between both methods suggests that GNSS provides accelerated processing without compromising precision.

Availability: Our observation period exceeding four hours was followed by a delay in post-processing via AUSPOS, due to their policy of processing data only after a minimum of 24-48hour latency period before processing newly collected data.

5. Conclusion and Recommendations

An evaluation of GNSS repeat measurement consistency was conducted, revealing that both approaches yield reliable results. Our research reveals that precise repeat observations can be achieved by comprehensively minimizing errors from other observable sources. In the context of deformation monitoring, exact repeat observation values are indispensable for reliably detecting and managing recurrent geodetic deformations. Consequently, it is advisable to conduct observations with meticulous attention to mitigating other observable errors that impact the precision of positional points.

Acknowledgement

We extend our sincere gratitude to the International GNSS Service (IGS) for providing access to the IGS-CORS dataset, instrumental to our research. Additionally, we acknowledge the invaluable support of AUSPOS's online processing service, which facilitated the processing of our observations using the advanced Bernese scientific software v.5.2 at no cost.

References

[1] Adjrad, M. and Groves, P. D. (2017**).** Intelligent Urban Positioning: Integration of Shadow Matching with 3D-Mapping-Aided GNSS Ranging. *The Journal of Navigation*, 71(1).

[2] Agrotis, L., Caissy, M., Weber, G., Hernandez-Pajares, M. and Hugentobler, H., (2012), The International GNSS Real-Time Service, GPS World.

[3] Ahmed, E., Manoj, D. and Nobuaki, K. (2017). Maintaining real-time precise point positioning during outages of orbit and clock corrections, GPS Solutions, DOI 10.1007/s10291-016-0583-4.

[4] Aldibaja, M., Suganuma, N., Yoneda, K. and Yanase, R. (2022). Challenging Environments for Precise Mapping Using GNSS/INS-RTK Systems: Reasons and Analysis. *Remote Sensing*. 14, 4058. https://doi.org/10.3390/rs14164058

[5] Altamimi, Z., Rebischung P., Métivier L. and Collilieux X. (2016), "ITRF2014: A new release of the International Terrestrial Reference Frame modelling nonlinear station motions", J. Geophys. Res. Solid Earth, 121, 6109–6131, doi:10.1002/2016JB013098.

[6] Ana, K. (2011). Precise Point Positioning (PPP) an alternative technique for ground base GNSS Tropospheric Monitoring. The institute of Geodesy and Geo-information of University of technology Gusshausstrasse, pp27-29.

[7] AUSPOS (cited 2023), (http://www.ga.gov.au/geodesy/sgc/wwwgps/), dated 26/10/2023.

[8] AUSPOS (cited 2024), (http://www.ga.gov.au/geodesy/sgc/wwwgps/), dated 22/07/2024.

[9] Bahadur, B. and Nohutcu, M. (2020). Impact of observation sampling rate on Multi-GNSS static PPP performance. *Survey Review*, 53, http://dx.doi.org/10.1080/00396265.2019.1711346.

 ISSN: 2354-3361
VOL. 2, ISSUE 1, PP 189–205, 2025 DOI: https://doi.org/10.5281/zenodo.14947243
PUBLISHED 28-02-2025
www.journals.unizik.edu.ng/jsis

[10] Colombo, O.L. (2008). Real-time, wide-area, precise kinematic positioning using data from internet NTRIP streams. In: Proc. ION-GNSS-2008. Institute of navigation, Savannah, Georgia, 327–337.

[11] El-Diasty, M. and Elsobeiey, M., (2015), Precise Point Positioning Technique with IGS Real Time Service (RTS) for Maritime Applications, http://www.scirp.org/journal/pos.

[12] El-Mowafy, A. (2011). Analysis of Web-Based GNSS Post-Processing Services for Static and Kinematic Positioning Using Short Data Spans. Survey Review, 43, 535-549. http://dx.doi.org/10.1179/003962611x13117748892074.

[13] Elsobeiey, M. and Al-Harbi, S. (2015). Performance of Real-Time Precise Point Positioning Using IGS Real-Time Service. GPS Solutions, 1-7. http://dx.doi.org/10.1007/s10291-015-0467-z.

[14] El-Mowafy, A., Deo, M. and Kubo, N. (2019). Maintaining real-time precise point positioning during outages of orbit and clock corrections. GPS Solution, Volume21, https://link.springer.com/article/10.1007/s10291-016-0583-4.

[15] Ge, M., Chen, J., Dousa, J., Gendt, G., and Wickert, J. (2011). A Computationally Efficient Approach for Estimating High-Rate Satellite Clock Corrections in Realtime. *GPS Solution.* 16, 9–17. http://dx.doi.org/10.1007/s10291-011-0206-z.

[16] Ge, M., Douša, J., Li, X., Ramatschi, M., Nischan, T. and Wickert, J. (2012). A novel real-time precise positioning service system: global precise point positioning with regional augmentation. Journal of Global Positioning Systems, doi:10.5081/jgps.11.1.2.

[17] Geng, J., Teferle, F.N., Meng, X., Dodson, A. (2010). Towards PPP-RTK: ambiguity resolution in real-time precise point positioning. Advances in Space Research. 47, 1664–1673. http://dx.doi.org/10.1016/j.asr.2010.03.030

[18] Griffiths, J. and Ray, J.R. (2009). On the precision and accuracy of IGS orbits. Journal of Geodesy, Volume 83, doi:10.1007/s00190-008-0237-6.

[19] Gurtner, W. and Estey, L. (2009). The Receiver Independent Exchange (RINEX) Format Version 3.01, Technical Report, UNAVCO.

[20] Hadas, T. and Bosy, J., (2015), Journal on IGS RTS precise orbits and clocks verification and quality degradation over time.

[21] Ju, B., Jiang, W., Tao, J., Hu, J., Xi, R., Ma, J. and Liu, J. (2022). Performance evaluation of GNSS kinematic PPP and PPP-IAR in structural health monitoring of bridge: Case studies GNSS Research Center, DOI:10.1016/j.measurement.

[22] Katrin, H., Florian, H., Christopher, A., Ana, K., Robert, W. and Philip, B. (2010). PPP: Precise Point Positioning – Constraints and Opportunities, Austria.

[23] Labrador, V. (2024). *satellite communication*. *Encyclopedia Britannica*. https://www.britannica.com/technology/satellite-communication, Accessed 25 September 2024.

[24] Li, X., Ge, M., Dousa, J. and Wickert, J. (2014). Real-time precise point positioning regional augmentation for large GPS reference networks. GPS Solutions 18(1): 61–71. DOI:10.1007/s10291-013-0310-3.

[25] Li, T., Zhang, H., Gao, Z., Chen, Q. and Niu, X. (2018). High-Accuracy Positioning in Urban Environments Using Single-Frequency Multi-GNSS RTK/MEMS-IMU Integration. *Remote Sensing*, 10(2), doi:10.3390/rs10020205.

[26] Lou, Y., Zhang, W., Wang, C., Yao, X., Shi, C. and Liu, J. (2014). The impact of orbital errors on the estimation of satellite clock errors and PPP. *Advances in Space Research*, (54) 8: 1571-1580. https://doi.org/10.1016/j.asr.

[27] Madimarova, G., Nurpeissova, T., Ormambekova, A., Suleimenova, D. and Zhildikbayeva, A. (2023). Advanced topographic-geodetic surveys and GNSS methodologies in urban planning, *Journal of Applied Geodesy*. https://doi.org/10.1515/jag-2023-0088.

[28] Manoochehr, S. and Thomas, R. W. (2011). Estimating the Effect of Satellite Orbital Error Using Wavelet-Based Robust Regression Applied to InSAR Deformation Data. *IEEE Transactions on Geoscience and Remote Sensing*, (49)11: 4600 – 4605. DOI: 10.1109/TGRS.2011.2143419

[29] Kamil, K., Radoslaw, Z. and Krzysztof, S. (2020). Evolution of orbit and clock quality for real-time multi-GNSS solutions, GPS Solutions (2020) 24:111, https://doi.org/10.1007/s10291-020-01026-6.

[30] Krzysztof, S., Radosław, Z., Grzegorz, B., Jarosław, B., Michael, M. and Salim, M. (2020). Quality assessment of experimental IGS multi-GNSS combined orbits, GPS Solutions, https://doi.org/10.1007/s10291-020-0965-5.

[31] Loyer, S., Perosanz, F., Mercier, F., Capdeville, H. Marty, J.C. (2012). Zero difference GPS ambiguity resolution at CNES-CLS IGS Analysis Center. Journal of Geodesy, https://doi.org/10.1007/s00190-012-0559-2.

ISSN: 2354-3361
VOL. 2, ISSUE 1, PP 189–205, 2025 DOI: https://doi.org/10.5281/zenodo.14947243
PUBLISHED 28-02-2025
www.journals.unizik.edu.ng/jsis

[32] Mervart, L. and Weber, G. (2011). Real-time combination of GNSS orbit and clock correction streams using a Kalman filter approach. Institute of Navigation, Portland, OR, USA, pp707–711.

[33] Patel, A. (2024). Modernizing Field Surveying: The Role and Impact of GNSS-RTK Technology in Digital Mapping. *Journal of Computer Technology and Software*, *3*(1), 1–4.

[34] Shi, J.B., Xu, C.Q., Guo, J.M. and Gao, Y. (2015). Real-time GPS precise point positioning-based precipitable water vapor estimation for rainfall monitoring and forecasting. IEEE Transactions on Geoscience and Remote Sensing. http://dx.doi.org/10.1109/TGRS.2014.2377041

[35] Vynohradenko, S., Siedov, A., Trehub, M., Zakharchenko, Y.and Trehub, Y. (2022). Features of Providing Engineering and Infrastructure Objects with Geospatial Information. *Review of Economics and Finance*, 20, 639-646 639.

[36] Weber, G., Mervart, L., Lukes, Z., Rocken, C. and Dousa, J. (2007). Real-time clock and orbit corrections for improved point positioning via NTRIP. In: Proc. IONGNSS-2007, Fort Worth, TX, 1992–1998.

[37] Yuan, Y. (2015). Real-time Retrieval of Precipitable Water Vapour from GNSS Precise Point Positioning, School of Mathematical and Geospatial Sciences, College of Science Engineering and Health, RMIT University, China.

[38] Zumberge, J.F., Heflin, M.B., Jefferson, D.C., Watkins, M. M. and Webb F. H. (1997). Precise Point Positioning for the Efficient and Robust Analysis of GPS Data from Large Networks. *Journal of Geophysical Research.*102 (B3), 5005–5017.